Hemp proteins conjugated with green tea polyphenol extract form *de novo* plant-sourced emulsifiers suitable for nanodelivery systems bearing lipophilic psychopharmaceuticals

William Charles Hosie,[1] Mary Augustina Egbuta,[1] Kasra Razmkhah,[1] Behzad Bolandi,[1†] Khalilalrahman Dehvari,[1†] Anton Homon,[1] Aleena Kappadakunnel,[1] Jonathan J. Simone,[2] Abhinandan Banerjee,[1,3*] John F. Trant[1,4,5,6*]

[1] Department of Chemistry and Biochemistry, University of Windsor, 401 Sunset Ave., Windsor, ON, N9B 3P4, Canada.

[2] Department of Biological Sciences, Brock University, 1812 Sir Isaac Brock Way, L2S 3A1

[3] Present address: Department of Chemistry, Colorado State University, Centre Ave, Fort Collins, CO, 80523, United States of America.

[4] Department of Biomedical Sciences, University of Windsor, 401 Sunset Ave., Windsor, ON, N9B 3P4, Canada.

[5] Binary Star Research Services, LaSalle ON, N9J 3X8, Canada.

[6] WE-Spark Research Institute, 401 Sunset Ave., Windsor, ON, N9B 3P4, Canada.

[†] These authors contributed equally to the work and are listed in alphabetical order only as a non-biased method. The two authors may invert the order for any professional purpose.

* Corresponding authors' email addresses:
abhinandan.banerjee@colostate.edu;
j.trant@uwindsor.ca.

Abstract

Nanoformulation is often used to improve the solubility and uptake of bioactives; however, it also protects sensitive bioactives from chemical decomposition. We report a class of biocompatible emulsifiers created by conjugating hemp protein with green tea polyphenols. A simple pH-assisted coupling protocol was employed to synthesize covalent and non-covalent conjugates, which were then used to produce 5-methoxy-*N*,*N*-dimethyltryptamine (5-MeO-DMT) enriched hemp oil nanoemulsions in water with an average droplet sizes of *ca.* 200 nm and ζ potential values of *ca.* -40 mV. Our *de novo* emulsifiers protected the sensitive drug under conditions of simulated oxidative stress, an indication that the antioxidant properties of polyphenols are retained. These emulsions were resistant to a wide variety of emulsion-breaking stressors and demonstrated remarkable colloidal stability over a period of 4 weeks with no evidence of phase separation. Fluorescence and confocal imaging confirmed cellular uptake of the formulation, while *in vitro* cytotoxicity assays showed acceptable cell viability with drug-loaded nanoemulsions. This represents an ingestible 5-MeO-DMT formulation; the sensitivity of this molecule mandates some form of formulation for reasonable bioavailability and reproducible dosages.

Keywords: psychedelic; nanoemulsion stability; cellular uptake; stress testing; rapid release, 5-MeO-DMT

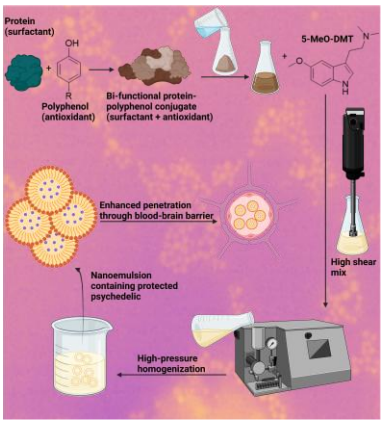

Green tea polyphenols, conjugated either covalently or non-covalently to hemp protein comprise an excellent stabilizing matrix for oxidatively-sensitive small molecules. These food-grade nanoemulsions are highly stable to a variety of chemical and physical stressors protecting the small molecule, while allowing for easy uptake across cell membranes, and rapid release once extensively diluted, providing a promising technology for oral delivery.

Introduction

With recent changes in cultural attitudes driving a review of the prohibitive regulations around psychoactives, clinicians are investigating the potential of compounds such as tetrahydrocannabinol,[1] cannabidiol,[2] psilocybin,[3] mescaline,[4] dimethyltryptamine (DMT),[5-9] cannabis-derived terpenes,[10-13] and lysergic acid diethylamide (LSD)[14, 15] for treating treatment-resistant depression & major depressive disorder,[16-18] substance use disorder,[19, 20] and neurodegenerative disorders.[21] However, any pharmaceutical application requires both precise dosing and a mitigation of person-to-person variance in effects. The short shelf-life, stress-induced, first-pass metabolism & enzymatic degradation, limited bioavailability, and limited solubility in biological fluids necessitate the careful design of functional formulations of these bio-actives to be effective and have the potential for regulatory approval.[7],[22] 5-MeO-DMT is a highly selective 5-HT_{1A} agonist.[23, 24] It stimulates neurogenesis (in mice)[25, 26] [27]and has a long-lasting anti-anxiety and anti-depressant effect from a single dose. It also has systemic effects on neuroendocrine, inflammatory, and immunoregulatory processes, and is an exceedingly promising potential therapy for serious mental distress; however, its pharmacology is not completely understood.[23, 24]

A recent clinical trial of a vaporizable form of 5-MeO-DMT (GH Research PLC, Dublin, Ireland) was published detailing the efficacy of 5-MeO-DMT for treatment-resistant depression but required three daily doses of *in situ* produced 5-MeO-DMT aerosols for successful biological uptake;[28] several adverse drug reactions were reported in the study which are more associated with the dosing form rather than the drug itself. Another 5-MeO-DMT intranasal spray has entered phase IIa clinical trials (Beckley Psytech Ltd., Oxford, UK); this involves a single inhalable dose of 5-MeO-DMT, is well-tolerated, and produces a sustained antidepressant outcome for 3 months.[29] While no serious adverse events were observed, mild nasal discomforts were reported possibly linked to the use of NaOH in the nasal formulation. Nevertheless, we note that the stated formulation may also lead to active pharmaceutical ingredient (API) degradation *in situ* due to the alkalinity of the storage solution. In any case, neither “formulation” encapsulated the API to facilitate transmucosal uptake in the nose (bypassing the blood-brain barrier), and instead both seek a simple introduction of the unmodified polar API into the bloodstream.[30] An intranasal nanoencapsulated formulation would solve several issues: it would bypass the first pass

metabolism, ensure direct uptake into the brain, and allow for a significant decrease in the dose lowering off-target systemic effects.[31-33] By evading several barriers, this would also likely decrease interpersonal variation and give a more controlled dose.[31, 34, 35]

Proteins are an inherently biocompatible solution for physically stabilizing colloidal dispersions and chemically protecting the APIs within.[36],[37] Plant proteins conjugated to green tea polyphenols (GTPs) represent a relatively new subclass of functional emulsifiers.[38],[39],[40],[41],[42] Polyphenols, which contain one or more aromatic rings bearing phenolic hydroxyl groups, are antioxidant, antimicrobial, antimutagenic, and anti-inflammatory secondary metabolites found in various plants.[43, 44] A conjugate of polyphenols and proteins could provide an antioxidant colloidal stabilizer comprised entirely of generally-recognized-as-safe (GRAS) materials,[45] facilitating regulatory approval.[46]

Proteins and phenols can be conjugated either physically or chemically. The former involves simple entropically-driven absorption through the formation of a multivalent network of non-covalent interactions between the partners.[47] Alternatively, the components can be (non-specifically) ligated through free radical grafting, electrophilic trapping or alkaline coupling.[48] The covalent conjugates are more stable than their non-covalent counterparts, but both have proven sufficiently stable to be used for both pharmaceutical- and nutraceutical delivery,[49] with applications spanning fish oil emulsions, β-carotene emulsions and the chemotherapy doxorubicin.[50],[51],[52] In this work, we synthesized, characterized and employed both covalent and non-covalent conjugates of hemp protein and green tea polyphenols as stabilizing carriers for 5-methoxy-dimethyltryptamine (5-MeO-DMT) to form both a non-covalent conjugate emulsion (NCCE) and a covalent conjugate emulsion (CCE). The resulting nanoemulsions (NEs) were characterized colloidally throughout a wide battery of physical and chemical stress tests. Their cytotoxicity was evaluated as well as the formulations' ability to permeate glioblastoma (GBM) cells to demonstrate cellular uptake.

Experimental Methodology

Materials and Reagents

The hemp protein used was purchased from Manitoba Harvest Hemp Foods (Tilray, New York, NY, USA). The hemp oil was purchased from Nature's Oil (Aurora, OH, USA). Green tea polyphenols (green tea extract, 98% tea polyphenols) were purchased from Creative Enzymes

(Upton, NY, USA). All the above agents are food-grade. Corn oil and Tween 80 were purchased from Charles Tennent and Company Ltd. (North York, ON, Canada). HPLC-grade water (EMD Millipore, Burlington MA, USA) was used in all experiments. Sodium azide, $CaCl_2$ and sucrose were purchased from Sigma Aldrich (St. Louis, MO, USA). Sodium dodecyl sulfate (SDS) was purchased from AK Scientific (Union City, CA, USA). 4′,6-diamidino-2-phenylindole (DAPI) was purchased from Aaron Chemicals (San Diego, CA, USA). Alexa Fluor phalloidin was obtained from Invitrogen (Eugene, OR, USA). 5-MeO-DMT, an unregulated psychedelic in Canada, was synthesized in the Trant lab, please see Supporting Information (SI), Section S4.[53] The Trant lab at the University of Windsor has a license from Health Canada allowing us to work with specific regulated materials; however we note that none of the materials used herein are regulated under Canadian law when this research was conducted.

General Protocols

Measurements of pH were conducted using a freshly calibrated, according to the manufacturer's instructions, pH meter (Milwaukee MW102 PRO+). All water used is HPLC grade, unless otherwise stated. All cell lines were obtained from the American Type Culture Collection (ATCC), except the U251 cell line was purchased from Glow Biologics (Tarrytown, NY, USA). Further details of experimental protocols are provided in the Supporting Information.

Synthesis of hemp protein-green tea polyphenol conjugates

Synthesis of HP – GTP_{cov}

Separate aqueous suspensions of hemp protein (HP, 8 g, 300 mL HPLC grade H_2O) and green tea polyphenols (GTP, 4 g, 200 mL HPLC grade H_2O) were prepared and adjusted with 0.1 M NaOH to pH 9. The protein solutions were allowed to solubilize at room temperature with stirring at 1500 rpm in a closed round-bottom flask over 24 hours to ensure maximum solubility, and 0.375 wt% sodium azide (of the weight of protein) was then added. The GTP solutions were prepared fresh at this 24-hour mark as the polyphenols are readily soluble in water. The protein solution was then subjected to probe sonication (Vevor, Ultrasound processor, 20 kHz, 300 W, model: CSBJZQFS-300N0001V1) at 80% power for 10 minutes with cycles of 40 seconds on, and 20 seconds off. The

protein solution was then immediately added to the GTP solution while maintaining the pH of the mixture at 9 with 0.1 M NaOH. The mixture was then allowed to react for 48 hours at room temperature, open to the atmosphere, with stirring at 1500 rpm. Then the mixture was dialyzed (3.5 K MWCO Snakeskin dialysis tubing) against water for 2 days with the water changed every 2 hours each day (a total of 18 changes). Dialysis was considered complete when the UV-visible absorption of the dialysate was found to be less than 0.01 between 350 and 450 nm (10 mm path length, no dilution), indicating that minimal free polyphenols were still being released. The dialyzed product was then lyophilized (Labconco, Freezone 4) for 48 hours with the chiller set to a temperature of -50 °C and a pressure of <1 mbar to produce a milky-brown solid.

Synthesis of HP – GTP_{noncov}

The HP – GTP_{noncov} was created using an identical procedure, except all steps were conducted at pH 7, and the mixture was purged with nitrogen gas for 30 mins before—and then stirred under a nitrogen atmosphere during—the 48-hour incubation period. The dialysis and lyophilization followed the same procedure. All conjugates were then stored in screw-topped glass vials on the benchtop with no particular efforts to exclude oxygen or moisture.

Determination of emulsion stability and emulsion activity indices (ESI and EAI)

Determination of the ESI and EAI was carried out in accordance with the method of Chatterjee *et al.*, with slight modifications.[54] A mixture of corn oil and 1% (w/v) protein conjugate solution in a 1:3 ratio at pH 7 was subjected to high-shear mixing with a rotor-stator (IKA T18 digital) at a speed of 7000 rpm for 10 minutes. A 50 µL aliquot of the emulsion was sampled both immediately (A_0) and 10 minutes (A_{10}) after the emulsion was formed. 5 mL 0.1% (w/v) sodium dodecyl sulfate (SDS) was added to the aliquots and mixed well. The absorbances of the SDS-treated emulsions were measured at 500 nm using a spectrophotometer (Hewlett Packard, 8452A, diode array) and the amplitude was used to calculate the EAI & ESI using the following formulae:

1.1 $$EAI\ \left(\frac{m^2}{g}\right) = \frac{(2 \cdot 2.303 \cdot A_{500\ nm})}{(F \cdot protein\ weight\ (g))}$$

where F is the oil volume fraction, and

1.2 $$ESI\ (min) = A_o \cdot \frac{\Delta t}{\Delta A}$$

where $\Delta t = 10\ min$ and $\Delta A = A_O - A_{10}$.[54]

Preparation of 5-MeO-DMT nanoemulsions

To prepare oil-in-water (O/W) NEs of 5-MeO-DMT stabilized by the HP – GTP conjugates, we used our method previously reported for a saponin formulation, with some modifications.[55] A round-bottom flask equipped with a stir bar was charged with 5-MeO-DMT (0.4 wt% of the final concoction) and a requisite amount of hemp oil (2 wt% of the final concoction) under an N_2 atmosphere. The solution was heated in a water bath at 65 °C to ensure the complete dissolution of 5-MeO-DMT in the hemp oil. The aqueous phase was prepared by adding the requisite amount of HP – $GTP_{noncov/cov}$ surfactant (2 wt% of the final concoction) along with any secondary surfactant (*e.g.* Tween 80, 0.4 wt%) to HPLC grade water (95.2 wt%). This aqueous phase was then centrifuged at 2500 rpm for 5 minutes (VWR® Centrifuge with 15 mL rotor, 76019-132) and the supernatant was retained; this removed any insoluble protein aggregates. The two phases were then combined and mixed using a rotor-stator mixer (IKA T18 digital) at 10,000 rpm for 3 cycles of 60 sec on, and 60 sec off to avoid excessive internal heating. The resulting coarse emulsion was then placed in the high-pressure homogenizer (Nano DeBee, BEE International, USA) and homogenized at a pressure of 20,000 – 25,000 psi in five sequential cycles using the Z8 nozzle with an aperture size of 0.20 mm. The resulting brown solutions of the NEs were then kept in sealed transparent vials at ~4 °C for long-term storage. The 5-MeO-DMT NE formed from HP – GTP_{noncov} is referred to as the non-covalent conjugate emulsion (**NCCE**), while that formed from HP – GTP_{cov} is referred to as the covalent conjugate emulsion (**CCE**)

Preparation of Nile red 5-MeO-DMT nanoemulsions

For the preparation of Nile Red-doped NEs, 1 $mg{\cdot}g^{-1}$ of Nile Red, with respect to the final concoction, was added into the oil phase at the same time as the 5-MeO-DMT. The rest of the process was conducted as described above.

Determination of emulsion particle size (droplet size) and distribution analysis

The stability and quality of the NEs were quantified by measuring the average solvodynamic radius particle size (d_z) and particle size distribution (PDI) of the droplets. This analysis was carried out by dynamic light scattering (DLS), also known as photon correlation spectroscopy, using a Zetasizer (Nano ZS, Malvern Instruments Ltd., UK). Emulsions were diluted 100-fold with HPLC-

grade water to avoid multiple scattering immediately prior to measurement. Applying the auto-correlation function on the intensity of light scattered from the particles allows the d_z to be calculated. The software (Zetasizer Software 8.01) employed was supplied by the manufacturer and disposable poly(styrene) cuvettes (ZEN0040) were used for all measurements. For further details, please see Supporting Information ***S7.5***.

Stress Tests

Stability upon long-term storage

The effect of long-term storage on the colloidal stability of the NEs was analyzed by storing them in transparent vials at 4 °C. Aliquots were taken every seven days for a period of 4 weeks.

Stability through freeze-thaw cycles

1 g of either CCE or NCCE was placed in a freezer at a temperature of -20 °C for 1 hour, then left on the bench at room temperature and allowed to completely thaw; the process was repeated with the same vial for two more cycles. Aliquots were sampled after each freeze-thaw cycle for DLS measurements.

Stability through flash heating

1 g of the NE (CCE or NCCE) was placed in a pre-heated water bath (80 ºC) and allowed to warm to that temperature and held at it for 1 minute. This process mimics an extreme case of the high-temperature–short-time pasteurization process (generally 71.5 °C for 15 seconds) used on milk and fruit juices during industrial production.[56] The NE was then allowed to cool to room temperature and an aliquot was taken for DLS and HPLC analysis.

Stability as a function of pH

3 g of the CCE or NCCE was placed in a vial, and the pH adjusted using either 0.1 M HCl or 0.1 M NaOH. The final masses of all aliquots were adjusted to the same amount with HPLC grade water to account for differences in the amount of acid or base added. The vials were then sealed and allowed to sit at 4 ºC for 12 to 18 h as indicated. Aliquots were then withdrawn for HPLC quantification of the 5-MeO-DMT and other aliquots of the samples were then diluted with pH-matched water for DLS analysis.

Stability upon the addition of salt, sugar, and a model preservative

$CaCl_2 \cdot 2H_2O$ (final concentrations 1 – 250 mM) were added to 5 mL portions of CCE or NCCE. To ensure complete dissolution of salt, the samples were vortexed for 60 seconds each. After 12 hours of incubation at 4 ºC, aliquots were taken for HPLC and DLS analysis. Dilution for DLS was done using isotonic solutions of $CaCl_2$. This same procedure was repeated for sucrose (1 – 500 mM) and potassium sorbate (K-sorbate, 2.5 – 15 mM).

Antioxidant capacity as measured by the DPPH assay

The 2,2-diphenyl-1-picrylhydrazyl (DPPH) solution was prepared by dissolving 7.9 mg of DPPH in 100 mL of anhydrous EtOH and was then kept in the dark at room temperature for at least 2 h. 1 mL of this DPPH solution was then added to a mixture containing 0.8 mL tris(hydroxymethyl)aminoethane-hydrochloride (Tris-HCl) buffer and 0.2 mL of the analyte solution. The solutions were mixed quickly before allowing to incubate in the dark for a further 30 min. At 30 minutes, the absorbance was recorded at 517 nm. The stock sample concentrations were made at 1.0 $mg \cdot mL^{-1}$ and serial dilutions were prepared to span a concentration range of 0.25 – 0.0125 $mg \cdot mL^{-1}$. A solution of 1 mL EtOH, 0.2 mL of water, and 0.8 mL Tris-HCl buffer was used as a blank for the absorbance. In the cases of a highly colored sample with background absorbance at 517 nm, a mixture of 1 mL EtOH, 0.8 mL Tris-HCl buffer, and 0.2 mL of each sample was used as a blank. The percentage radical scavenging of a sample is calculated from the following equation:

1.3 $$\% \, radicals \, scavenged = \left(\frac{A_1 - A_2}{A_1}\right) \cdot 100\%$$

where A_1 is the absorbance of DPPH with EtOH in place of the testing sample and A_2 is the absorbance of the sample being examined.

Cell culture

The rat lung cell line L2 was purchased from the American Type Culture Collection (ATCC, Rockville, MD, USA) and cultured in Dulbecco's Modified Eagle's Medium/Nutrient Mixture F-12 Ham (DMEM-F12, Sigma-Aldrich, St. Louis, MO, USA) supplemented with 10% fetal bovine

serum (FBS, Sigma-Aldrich) and 1% penicillin/streptomycin (Sigma-Aldrich). The human breast cancer cell line MDA-MB-231 was obtained from ATCC and cultured in Dulbecco's Modified Eagle's Medium (DMEM, Sigma-Aldrich) supplemented with 10% FBS (Sigma-Aldrich) and 1% penicillin/streptomycin (Sigma-Aldrich). The human glioblastoma cell line U87 was purchased from ATCC and cultured in Minimal Essential Medium with Earl's Balanced Salts (MEM/EBSS, HyClone, Logan, UT, USA) supplemented with 10% FBS (Sigma-Aldrich) and 0.5% penicillin/streptomycin (Sigma-Aldrich). The human glioblastoma cell line U251 was purchased from Glow Biologics (Tarrytown, NY, USA) and cultured in MEM/EBSS (HyClone, Logan, UT, USA) supplemented with 10% FBS (Sigma-Aldrich), 1% non-essential amino acids (NEAA, Sigma-Aldrich, UK), and 1% penicillin/streptomycin (Sigma-Aldrich). All cell lines were cultured at 37 °C in a 5% CO_2 atmosphere and 95% humidity; and subcultured upon reaching 70% confluency.

Evaluation of cytotoxicity

The cytotoxicity of the NEs was measured using the MTT (3-(4,5-dimethylthiazol-2-yl)-2,5-diphenyltetrazolium bromide) assay on four different cell lines: L2 rat lung, MDA-MB-231 human breast cancer, and U87 and U251 human glioblastoma cells [57]. Briefly, cells were seeded in 96-well microtiter plates (100 µL per well, including media) at the following densities: L2 cells, 1×10^3 cells/well; MDA-MB-231 cells/well, 2×10^3 cells/well; and U87 and U251 cells, 3×10^3 cells/well. After 24 hours of incubation at 37 ºC in a 5% CO_2 atmosphere with 95% humidity, cells were treated with 50 µL of the analyte at four different concentrations (275, 27.5, 2.75, and 0.275 $\mu g \cdot g^{-1}$). After 48 hours of incubation, the media was discarded, and 100 µL of 0.5 $mg \cdot mL^{-1}$ MTT stock solution was added to each well. The plates were incubated for an additional 4 hours at 37 °C under 5% CO_2 and 95% humidity. Following incubation, the MTT solution was discarded, and the resulting formazan crystals were solubilized with 100 µL/well of dimethyl sulfoxide (DMSO). Absorbance was measured at 570 nm using a microplate reader (SpectraMax M5e, Molecular Devices, USA). Cell viability (%) was calculated as the ratio of absorbance in treated cells to absorbance in control cells (untreated cells).

Fluorescence cellular imaging

Human glioblastoma U87 and U251 cells at a density of $1x10^6$ cells/ per well were seeded onto coverslips within the wells of a 6-well plate containing 2 mL of the MEM/EBSS (Hyclone)

complete media. Following this, the plates were incubated at 37 °C with 5% CO_2, and 95% humidity, allowing the cells to adhere and proliferate over a 24-hour period. Nile Red-loaded NEs were diluted with the growth medium to achieve specific concentrations: 1.44 $mg{\cdot}mL^{-1}$ for CCE and 1.14 $mg{\cdot}mL^{-1}$ for NCCE ensuring a final Nile Rred concentration of 40 $\mu g{\cdot}mL^{-1}$. Subsequently, the medium EMEM (MEM/EBSS Eagle's minimum essential media, Hyclone) was replaced with a fresh medium containing the respective NEs, and the cells were incubated for an additional 24 hours (37 °C, 5% CO_2). After incubation, the media was aspirated from each well, and the cells were washed with PBS to remove non-internalized NEs. The cells were then fixed using 4% paraformaldehyde for 15 minutes at room temperature. Following fixation, the cells were rinsed with PBS and stained with DAPI (1 *μg/mL*) for 20 minutes. Afterward, excess DAPI solution was removed by washing the cells with PBS. Finally, the coverslips containing the stained cells were mounted onto glass slides, imaged, and analyzed using a Leica CRT 6500 fluorescence microscope.

Confocal laser scanning microscope imaging

Human glioblastoma U87 and U251 cells at a density of 1×10^5 cells per well were seeded onto coverslips within the wells of a 6-well plate containing 2 mL of MEM/EBSS (Hyclone) complete media. The plates were incubated at 37 °C with 5% CO_2 and 95% humidity overnight. Nile Red-loaded NEs at a concentration of 0.07 *mg/g* were diluted 10 times with the growth medium and exposed to the cells by adding 1 mL to each well. Subsequently, the cells were incubated for an additional 24 hours (37 °C, 5% CO_2). After incubation, the media was aspirated from each well, and the cells were washed 3 times with PBS to remove non-internalized NEs. The cells were then fixed in 4% paraformaldehyde for 15 minutes and permeabilized with 0.2% Triton X-100 for 5 min at room temperature. Following, the cells were rinsed with PBS and the cytoskeleton were stained with phalloidin (1.25 *μg/mL*) and nucleus staining was performed using DAPI (1 *μg/mL)* for 30 min. Finally, the mounted cover slips on glass slides were observed and imaged with a Zeiss LSM900 confocal laser scanning microscope (LSM900, Jena, Germany).

Drug release kinetics

Kinetic release studies were conducted using the method described by Sood *et al.*, with some modifications.[58] 1 mL of the NE was loaded into a dialysis bag (10 K MWCO Snakeskin dialysis

tubing, Thermo Scientific™) and tightly closed with dialysis clips. The bag was then placed in 100 mL of dialysate containing phosphate buffer saline (pH 7.3) while maintaining a temperature of 37 °C (through direct measurement and temperature control of the heater-stirrer by a thermocouple probe inserted into the dialysate) and stirring at 100 rpm. 1 mL aliquots were taken at various time points between 0 (before inserting the dialysis bag) and 420 mins for HPLC quantification, and the dialysate was replenished to account for the volume loss upon sampling. The kinetic release data was then fitted using kinetic models such as zero-order, first order, Korsmeyer-Peppas, Higuchi, and Hixson to get better insight into the release mechanism of 5-MeO-DMT from within the NE droplets.

Determination of encapsulation efficiency (EE) and loading capacity (LC)

EE and LC were determined via the method described by Zielińska *et al.*, with some modifications.[59] This was done using filtered centrifuge tubes (Amicon® Ultra Centrifugal Filter) with a filter of 50 K MWCO (molecular weight cut off). Initially, 5 *g* of nanoemulsion (CCE or NCCE) is loaded into the centrifuge tube and spun at 1500 rpm for 25 minutes at 20 °C. The pellet and the supernatant are weighed and then 5-MeO-DMT content is quantified *via* HPLC. EE % is calculated using equation 1.4. and LC % is calculated using equation 1.5.

1.4 $$EE\ \% = \frac{W_{API} - W_S}{W_{API}} \cdot 100$$

1.5 $$LC\ \% = \frac{W_{API} - W_S}{W_{API} - W_S + W_L} \cdot 100$$

where W_{API} is the mass of API added to the formulation, W_S is the mass of API found in the supernatant, and W_L is the mass of lipid used in the formulation.

Statistical Analysis

Unless otherwise indicated, all experiments were performed in triplicate, data is represented as means ± standard deviation and the data was analyzed using either MS Excel or Origin Pro 8.5 graphing software (MA, USA). SPPS (IBM) was used for statistical analysis. All statistical analyses are reported dependent on Tukey's post-hoc test with Bonferroni corrections where appropriate.[60] According to the customs of the field, a p-value <0.05 is considered statistically significant.

Results and Discussion

Characterization of the de novo emulsifiers

After preparation and isolation, the conjugates were analyzed using a battery of both spectroscopic and thermal methods (**Figure 1**), as well as radical scavenging assays (**Figure 2**). The proposed mechanism of protein – polyphenol coupling is provided as Supplementary Information, Section S1.

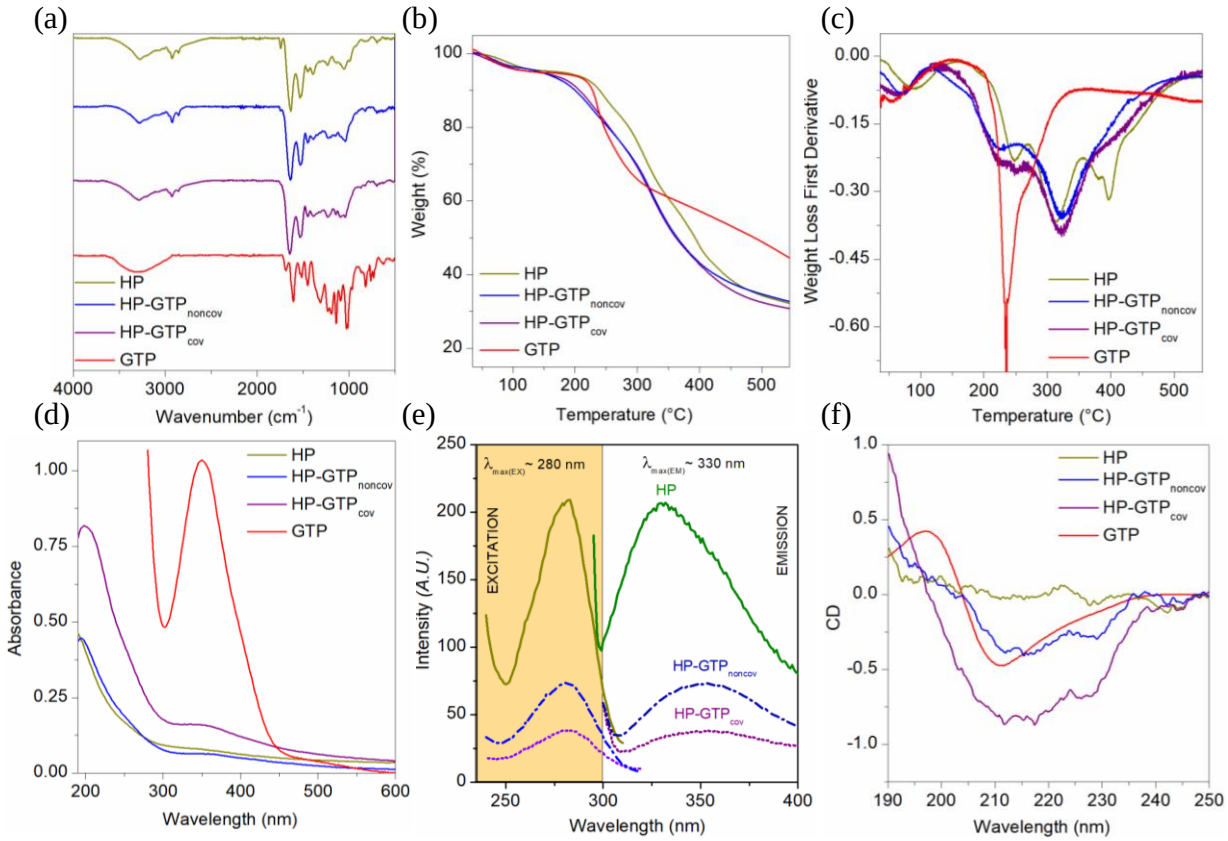

Figure 1. Collected physical characterization data for the complex conjugate emulsifiers: (a) ATR-IR (spectra has been baseline corrected and normalized to the most intense peak); (b) thermograms; (c) first derivative of the thermograms; (d) UV-visible spectra; (e) fluorescence spectra; and (f) CD spectra. Hemp protein (HP) is depicted in olive, green tea polyphenol (GPT) in red, the noncovalent conjugate (HP – GTP_{noncov}) in blue, and the covalent conjugate (HP – GTP_{cov}) in purple.

There is little difference in the IR spectra of HP – GTP_{noncov} and HP – GTP_{cov}, and this is as expected (**Figure 1a**); however, some points do deserve discussion. The presence of the GTP in HP – GTP_{noncov} can be deduced by the presence of more intense bands corresponding to phenolic stretches in the non-covalent conjugates around ~1350 cm^{-1}.[61] This is not observed in the covalent conjugates due to the use of sodium hydroxide as a catalyst to oxidize the phenols into quinones, which may not have been completely reduced after oligomerization and conjugation to protein heteroatoms. Thermograms and their first derivative plots (**Figure 1b** and **1c**) testify to the lower thermal stabilization of the conjugates compared to native HP. The water loss step ends 50 °C sooner for both HP – GTP conjugates, likely due to the processing releasing much of the tightly bound internal water present in the native protein. The conjugates lose more mass at lower temperatures than the protein itself: the polyphenol oils are more volatile than the native protein, leading to higher mass loss at lower temperatures—an onset temperature of between 200 and 250 ºC is typical for green tea polyphenols.[62] The large step around 315 °C is still present in both conjugates and accounts for the majority of the mass loss. This is consistent with the typical temperature range for the majority of the mass loss in protein-rich samples.[63] The thermogravimetric data is consequently consistent with a material containing both GTPs and HP. One would not expect a significant difference between a covalent and a non-covalent system here as the few linkages would not likely change thermal behaviour.

UV-visible spectroscopy (**Figure 1d)** reveals a small peak at 280 *nm* in the native HP, correlating with phenylalanine, tryptophan, and tyrosine residues.[64] The UV-visible spectrum of the GTP displayed a very intense peak at 350 *nm* which correlates to $n \rightarrow \pi^*$ electronic transition of catechins.[65] This peak is also present in both conjugates, albeit at lower intensity.

The emission fluorescence spectrum of the native HP is, as expected, much more intense than that of either of the conjugates (**Figure 1e**).[66] This result might be due to the participation of fluorophores such as tryptophan in HP participating in the formation process of HP – GTP conjugates, which would lead to fluorescence quenching; the close localization of polyaromatic phenols would also be expected to lead to fluorescence quenching via a through-space interaction as is generally seen in these types of systems.[67, 68] The covalency of HP − GTP_{cov} induced a greater fluorescent quench than the noncovalent counterpart. The λ_{max} of the emission spectrum after conjugation red-shifts from ~330 *nm* to ~352 *nm* in both of the conjugates. This shift is suggestive of denaturation of the protein tertiary structure, exposing more side chains to the bulk

solution.[69] The native GTP did not show any fluorescence at these wavelengths (data not shown). Additional discussion of the information gleaned from these individual physical characterization techniques may be found in the SI (see section S2).

The native HP exhibited a very poor, close to zero, CD signal, possibly due to the presence of small chiral impurities, such as sugars and phospholipids that one would expect in a commercial material (**Figure 1(f)**). During the synthetic process of the conjugates, the protein gets purified *via* dialysis, resulting in stronger CD signals as these impurities are removed. The negative signals at 210 and 225 *nm* and the positive one below 190 *nm* suggest a beta-sheet secondary structure for both conjugates. According to Guo *et al*., this could be due to the breaking of hydroxyl groups in stable α-helical structures to interact with green tea polyphenols, inducing β-sheet structures, but according to Bestsel CD analysis,[70] there is no meaningful α-helical structures in the native HP.[71] Deconvolution of the CD spectra suggests that there is little change in the hemp protein's secondary structure pre- and post- conjugation. The most significant change that is detected is an increase of anti-left-twisted β-sheets from 0.6% in the HP to 2.6% in HP – GTP_{noncov} and 3.3% in HP – GTP_{cov}. This data is corroborated by the FT-IR analysis in that the secondary structure of the hemp protein is largely unchanged post-conjugation whether non-covalent or covalently linked. For a continued discussion of the CD spectra, and tables of the deconvolution analysis, please see section S2.3 of the Supporting Information.

The values of the HP – GTP conjugates' emulsion indices suggest colloidal stability

Before using our conjugates to create 5-MeO-DMT-loaded emulsions, their emulsion stability and activity indices were quantified to ensure they were appropriate. The EAI (emulsion activity index) refers to the ability of an emulsion to emulsify a given volume of oil per amount of emulsifier,[72] and the ESI (emulsion stability index) refers to the ability of said emulsion to resist coalescence as a function of time. The results of the EAI analysis show that HP − GTP_{noncov} and HP − GTP_{cov} possess average emulsifier activities of 104.6 ± 18.7 $m^2 \cdot g^{-1}$ and 94.2 ± 6.7 $m^2 \cdot g^{-1}$, respectively, which makes them outstanding emulsifiers—typical values for proteins and protein isolates are more commonly around 20-30 $m^2 \cdot g^{-1}$.[50, 54, 73-75] As well as high emulsifier activity, HP − GTP_{cov} also showed high stability (228.2 min). Surprisingly, the HP − GTP_{noncov} also showed good stability (120 min). For context, both conjugates showed better properties than any of the protein-based emulsions described in previous reports cited above on both parameters. These appear to be highly suitable materials for this application.

The HP – GTP conjugates have potent antioxidant activity

Emulsions are generally made to improve the solubility of an API, but they can also stabilize an API. The tryptamines and related structures are extremely sensitive to oxidative degradation under neutral conditions, so formulation may protect them and extend their shelf life.[76-78] One of the obvious benefits of the polyphenol emulsifier is the presence of the GRAS polyphenol antioxidants that should help protect the API. The protective effect was consequently determined by one of the more common oxidation-stress assays. The 2,2-diphenyl-1-picrylhydrazyl (DPPH) assay is a rapid, simple, and inexpensive method of evaluation of a compound's ability to operate as a free-radical scavenger/antioxidant.[79] It can be easily misused as an assay aiming to show the *in vivo* activity of an antioxidant,[80-82] but in this case we are interested in the activity during storage, and it is perfectly appropriate for this situation. The native GTP material has a DPPH assay IC_{50} value of 65 $\mu g \cdot mL^{-1}$, no radical scavenging activity was detected in the native protein (Figure 2). Of the freshly prepared emulsifier material, HP – GTP_{noncov} and HP – GTP_{cov} show outstanding IC_{50} values of 227 $\mu g \cdot mL^{-1}$ and 226 $\mu g \cdot mL^{-1}$. The concentration of the conjugates within the formulations are *ca.* 0.54 $mg \cdot mL^{-1}$ for HP – GTP_{noncov} and *ca.* 0.74 $mg \cdot mL^{1}$ HP – GTP_{cov}. Compared to well established antioxidant plant extracts such as *T. pallida* leaves (IC_{50} = 9.2 $\mu g \cdot mL^{-1}$)[83], and papain hydrosylates (IC_{50} = *30,400* $\mu g \cdot mL^{-1}$)[54] our emulsifiers show a moderate radical scavenging ability. This outcome was corroborated by pro-oxidative stress tests on our formulations in comparison with unformulated API solutions**,** please see SI section S3.

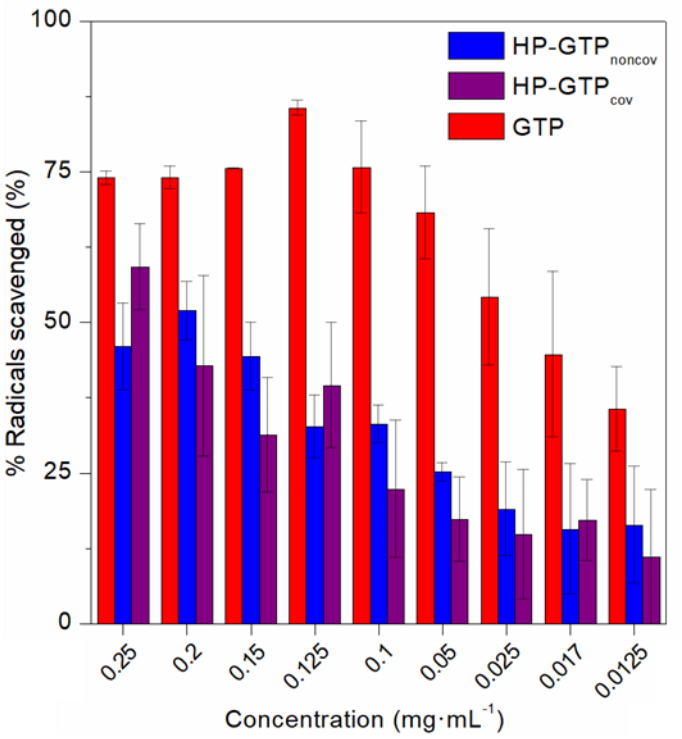

Figure 2. Radical scavenging activity of HP −GTP_{noncov} and HP −GTP_{noncov} as determined by the DPPH assay. Error bars are standard deviation of three experimental replicates.

Characterization and stress response analysis of 5-MeO-DMT NEs

Fingerprinting the freshly generated emulsions

Particle size analysis highlighted that these are textbook examples of NEs, with average droplet sizes under 250 nm, low to medium polydispersity, and very high zeta potentials (ζ), possibly owing to charged amino acid residues in the *de novo* emulsifiers (**Table 2**).[65],[84] It is to be noted that emulsions with ζ potential absolute values above 30 mV are considered highly stable owing to electrostatic droplet repulsion, a threshold that these emulsions cross easily.[85]

Table 2. Particle size, surface charge, and related parameters of the emulsions.

Emulsifier (emulsion)	Average droplet size (nm)	PDI	ζ_f (mV)	Peak shape
HP − GTP_{noncov} (NCCE)	200.2 ± 1.2	0.15	-39 ± 9.1	Gaussian
HP − GTP_{cov} (CCE)	203.6 ± 1.3	0.17	-43 ± 7.9	Gaussian

In the SEM micrographs, unlike the well-structured droplets visible for CCE (**Figure 3a**) and NCCE (**Figure 3b**), the control (5-MeO-DMT dissolved in hemp oil and diluted in hexane, **Figure S9**) showed large indistinct blobs which are tens of microns wide, clearly demonstrating the difference the formulation makes in terms of well-defined droplet formation and retention even after the SEM sample preparation protocol. The DLS sizes for these droplets are slightly larger than the SEM sizes; this is a well-known phenomenon common to all soft nanostructures arising from the drying of the sample onto a flat surface as required for SEM.[55, 85],[86]

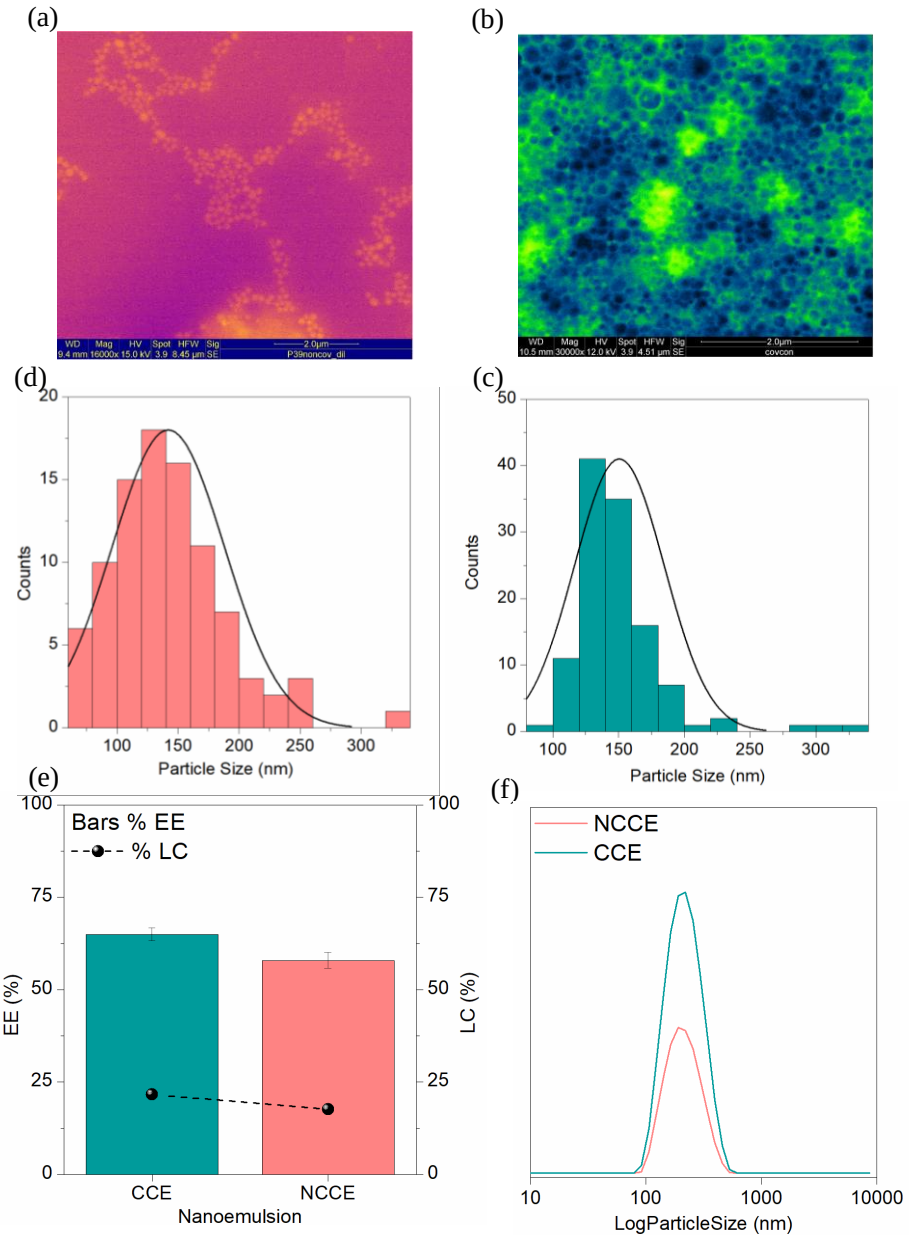

Figure 3. Top row: SEM images of (a) NCCE; (b) CCE. Middle row: SEM size distribution histograms of (c) NCCE and (e) CCE. Bottom row: encapsulation efficiency and loading capacity of (e) NCCE and CCE, lines connecting PDI dots are for visualization only; dynamic light scattering size distribution of (f) NCCE and CCE. NCCE is in salmon, CCE is in teal. Errors bars represent the standard deviation of three experimental replicates. SEM images were adjusted with color for increased visualization.

The NEs have moderate encapsulation efficiency (EE) and loading capacity (LC) for 5-MeO-DMT

The freshly prepared formulations were evaluated for EE and LC. EE is a measure of the percentage of the drug encapsulated within the NE droplets *vis-à-vis* the total drug content of the system including both the matrix-encapsulated fraction as well as the 'free-flowing' fraction that is in the outer aqueous environment. Loading capacity is the ability of the drug to be solubilized in the given amount of carrier oil. As shown in **Figure 3e**, the NCCE and CCE had an EE of 58 ± 2 % and 65 ± 2 %, respectively, with an LC of 17.6 ± 0.5 % and 21.6 ± 0.5 %. As 5-MeO-DMT has a calculated logP of approximately 1.7 some partition into both the aqueous and oil phases would be expected.

The NEs are stable to storage at 4 ºC

Storing the materials at 4 °C over one month leads to no change in the stability of the API **(Figure 4a**) or the particle size in both formulations, and no significant particle size or PDI increase for both the NCCE and CCE (**Figure 4b and 4c**). No visible phase separation, flocculation, creaming, sedimentation, or other emulsion destabilizing phenomena are noted for either.[87] This kind of stability is expected for our *de novo* emulsifiers because of their charged amino acid side chains leading to potent electrostatic inter-droplet repulsion.[64],[61] This indicates that the formulations show satisfying colloidal stability over a long period of time, making them suitable for commercial preparations.

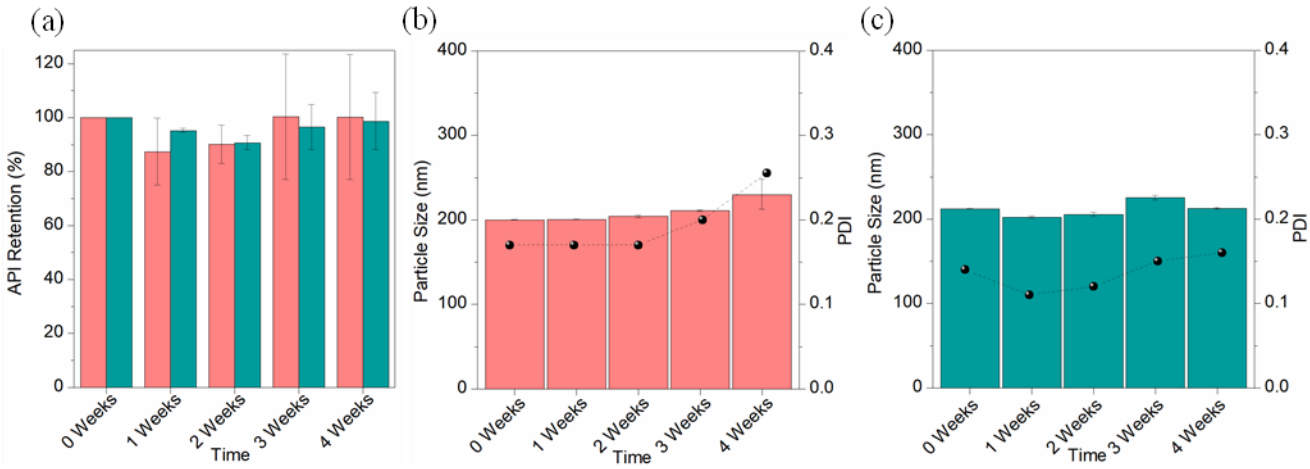

Figure 4. API retention of NCCE and CCE (a) and colloidal stability of NCCE (b) and CCE (c) over four weeks of storage in a fridge at 4 ˚C. The bars represent particle size, the spheres represent the PDI. NCCE is in salmon, CCE is in teal. Lines connecting PDI dots are for visualization only. Error bars represent the standard deviation of two experimental replicates.

The NEs are resistant to a wide variety of physical and chemical stressors

A round of flash pasteurization seems to only minimally increase the average droplet sizes and PDI for CCE and NCCE (Table 2), but they cannot be frozen: a single freeze-thaw cycle leads to a 10-fold increase in average droplet sizes and a drastic increase in PDI. Since NEs are kinetically rather than thermodynamically stable systems,[85] removal of kinetic energy through freezing destabilizes the emulsions, as expected. Heating 5-MeO-DMT to 85 °C for 60 seconds as a solution in *iso*-propanol (in a sealed tube) lead to a negligible concentration decrease of 3 ± 1 %.

Table 2: Colloidal properties of the NEs upon application of physical stressors.

System	Stressor	Particle Size (nm)	PDI
NCCE	As-is	200 ± 1	0.15
NCCE	Flash heating	207 ± 2	0.14
NCCE	Freeze-thaw cycle	1300 ± 560	0.19
CCE	As-is	204 ± 1	0.11
CCE	Flash heating	209 ± 2	0.13
CCE	Freeze-thaw cycle	2280 ± 150	0.85

Effect of additives

Chemical additives can have a profound effect on the stability of a nanoformulation (**Figure 5**).[88] However, the addition of sucrose up to 500 mM had no effect on the particle size for either the NCCE or the CCE. Neither did the addition of the ionic potassium sorbate, a common preservative. This was unexpected as we anticipated a destabilization of the emulsions due to growing disparity between the density and viscosity of the aqueous and lipid phases as more solute is dissolved in the aqueous phase.[85]

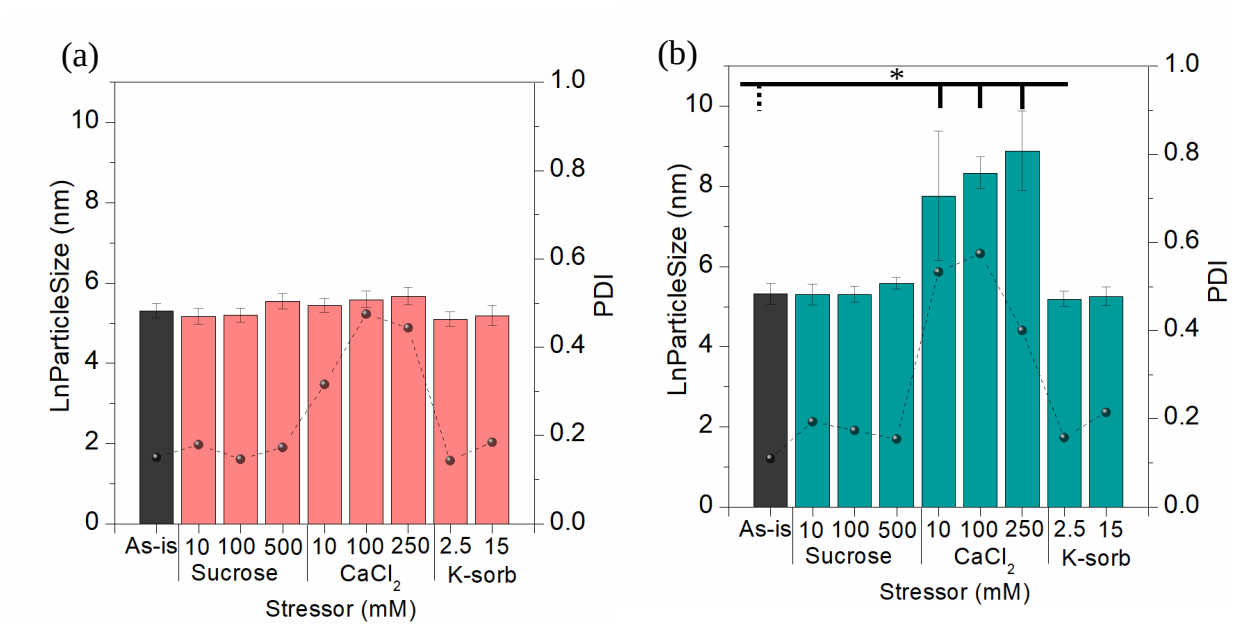

Figure 5. Particle size (bars) and PDI (spheres) in NCCE (a) and CCE (b) upon exposure to additives. Native properties; NCCE (avg droplet size = 200 nm, PDI = 0.15), CCE (avg droplet size = 204 nm, PDI = 0.17). NCCE is in salmon, CCE is in teal. Lines connecting PDI spheres are for visualization only. Error bars represent standard deviation of three experimental replicates. * $P < 0.05$. Solid vertical lines indicate samples are identical to each other but significantly different from the hashed line. Data is represented as the natural log of particle size for ease of visualization.

The addition of $CaCl_2$ was intended to mimic the effect of diluting with hard water, or the addition of essential minerals.[89] The addition of divalent cations often leads to instability and phase separation in NEs containing charged emulsifiers.[90] This effect is observed here in the CCE: there is an increase in adhesion to surfaces, and the consistency becomes thicker, potentially

owing to bridging interactions between the cation and the charges on the emulsifier. With the addition of 10 mM calcium chloride ($CaCl_2$) the CCE immediately destabilized, and particles aggregated to sizes >5 µm. The primary reason for this effect is that Ca^{2+} reduces the interdroplet Debye screening length, and consequently the interdroplet repulsion. If the effect is strong enough, the droplets come close enough that attractive interactions between them (such as van der Waal forces) predominate, leading to droplet coalescence and/or flocculation.[85] This effect of polyvalent cation additives is known to be especially strong in emulsions with ζ-potentials above 25 mV, as is the case here.[85],[90] This effect is not observed for the NCCE although we note an increase in dispersity. None of the chemical additives lead to any significant degradation of the API within the NEs (**Figure S12**).

Changes in pH can protonate or deprotonate terminal functional groups of emulsifiers, thereby modulating interdroplet electrostatic repulsive forces, and ultimately affecting droplet coalescence rates.[91] Protonation of the terminal $–COO^-$ groups in protein side chains of $HP-GTP_{cov}$ and $HP-GTP_{noncov}$ leads to reduced interdroplet repulsion at lower pH values, while at higher (*i.e.*, alkaline) pH values alkaline hydrolysis of covalent bonds would lead to destabilization of the conjugate emulsifiers. Quantitative analysis of emulsions at extreme pH values (1- acidic, 11 - alkaline) led to chemical degradation of 5-MeO-DMT **(Figure 6**). Neither formulation showed any phase separation under highly acidic or alkaline conditions. The CCE showed no API degradation at pH 11 while the API in the NCCE degraded by 28%, and the unformulated API (in ethanol) degraded by 36%. Average droplet sizes of the CCE changed from 203.6 nm (pH 8.7) to 376.8 nm (pH 3); for the NCCE, no significant changes in colloidal stability were observed from highly acidic to alkaline pHs except at pH 1 where the particle size rose from 200.2 nm (pH 9.8) to 245.4 nm (pH 1). The formulations do not protect the API from pH-degradation and the NCCE even appears to accelerate degradation relative to unformulated API, but this does not involve a loss in integrity of the nanoemulsion.

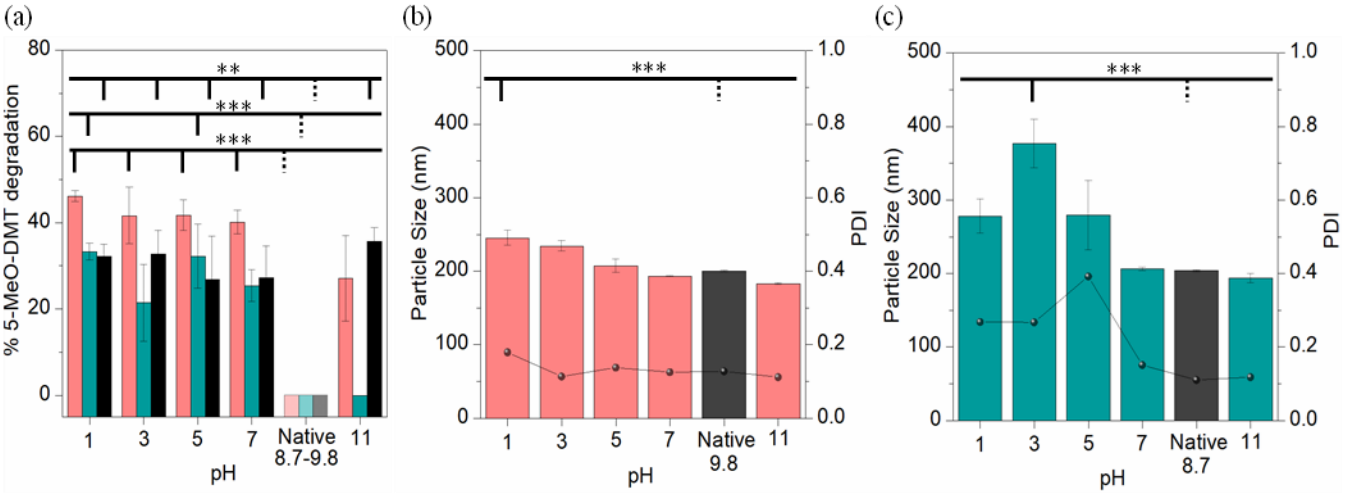

Figure 6. Evaluation of colloidal properties and API stability upon exposure to varying acidity or alkalinity: (a) 5-MeO-DMT concentration (black = unformulated 5-MeO-DMT in EtOH), particle size (bars) and PDI (spheres) in NCCE (a) and CCE (b), (c) CCE colloidal properties. Native pH: NCCE = 9.8, CCE = 8.7, Unformulated in EtOH = 9.4. NCCE is in salmon, CCE is in teal, and black is the unformulated drug. Lines connecting PDI spheres are for visualization only. Error bars represent standard deviation of three experimental replicates. ** $P < 0.01$, *** $P > 0.001$. Solid vertical lines indicate samples are identical to each other but significantly different from the hashed line

The comparably high stability of the NEs may be attributed to the fact that the creaming rate is directly proportional to the square of the droplet diameter—an emulsion with nanosized droplets, therefore, has a reduced rate of gravitational separation.[85] Additionally, Brownian motion effects that favor a homogeneous distribution of droplets throughout the system counteract the gravitational forces when the droplets are sufficiently small, as is the case for our nanoemulsions. The charged -COO^- termini present in the protein side chains of $HP-GTP_{cov}$ and $HP-GTP_{noncov}$ can also offer electrostatic stabilization by enhancing interdroplet repulsion. With respect to their chemical stability, the documented high free radical quenching capacity of protein-polyphenol conjugates minimizes oxidative degradation of the API 5-MeO-DMT within the CCE at pH 11.[92],[61] At any pH below 11, the API degradation in the unformulated sample *vs.* the NEs is not significantly different.

Kinetic release studies

Kinetic release studies were conducted to evaluate the rate at which 5-MeO-DMT is released from our formulations as well as to explore plausible drug release mechanisms applicable to our formulations (**Figure 7**). These NEs solve a key challenge associated with DMT-based 'free-base' drugs: their limited solubility in aqueous media or serum. After 150 minutes of dialysis, both the CCE and the NCCE release between 70 and 100% of the total drug payload, whereas the unformulated API suspension releases less than 15% after a period of 420 mins. This is not a slow-release formulation: the release kinetics are clearly diffusion-limited; however, this is not necessarily a problem. Psychedelics are generally taken unformulated for rapid onset, and although a slow release microdosing formulation likely has a role for some applications, fast release is likely preferred for mental health indications.

To determine the precise mode of release, several kinetic models (*i.e.* zero order, first order, Higuchi, Korsmeyer-Peppas, and Hixson-Crowell) were applied to the data. Going by the 'goodness of fit' parameters, the most likely mechanism of API release in these experiments seems to be rapid release of 5-MeO-DMT from the NEs over a period of minutes, followed by diffusion limited traversal of the API through the dialysis membrane, as evidenced by a high R^2 (0.988 for the CCE) value for the Higuchi model (**Figure S13**). This is in contrast with mechanisms typically seen in SNEDDS (self-nano-emulsifying drug delivery systems), loaded capsules where solvents would diffuse into the capsule shell's interior and induce capsule shell relaxation, followed by solubilization of the NE and drug release.[93] For both the CCE and the NCCE, at the 30-minute mark, approx. 50% cumulative drug release is already achieved. Again, this seems to indicate a rapid/'burst' release of the API from within the NE droplets, followed by a cumulative release to the outer medium whose rate is linear with respect to the square root of time ($\sqrt{t}$). This indicates that the rate of release arises due to the slow diffusion of 5-MeO-DMT across the membrane and its low solubility in the dissolution medium (<10 $mg{\cdot}mL^{-1}$).[78] We hypothesize that it takes time for the drug incorporated in the oil phase to be released even after the NE falls apart.[94] A high linearity [R^2 = 0.963; k_0 = 0.34 h^{-1} for CCE] for the zero-order kinetic fitting of our API release data implies a linear 5-MeO-DMT molecular release from within the dialysis bag. Zero-order release profiles are the direct consequences of the Fickian diffusion of the drugs through a membrane. We speculate that the initial rapid build-up of API outside the dialysis bag (which slows down eventually) may be due to the transfer of some of the NE through the dialysis

membrane, carrying the API with it. However, the NE droplets rapidly degrade within the dialysis bag, and the efficiency of 5-MeO-DMT crossing the membrane barrier then decreases as it corresponds to a diffusion-limited process. In contrast the unformulated API simply precipitates in the bag and does not dissolve at any meaningful rate.

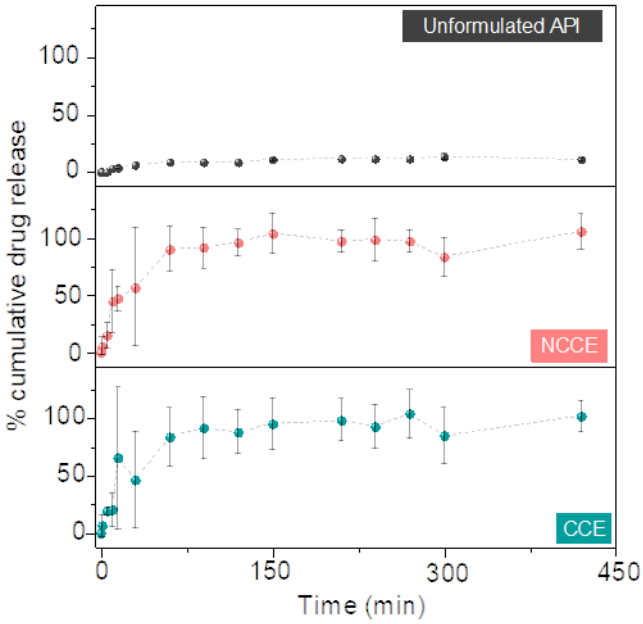

Figure 7. A comparative 5-MeO-DMT release profile of the two payload-bearing NE systems vis-à-vis unformulated 5-MeO-DMT. NCCE is in salmon, CCE is in teal. Error bars represent standard deviation of three experimental replicates. Lines connecting spheres are for aiding visualization only by guiding the eye and do not imply interpolated values.

The NEs moderate the toxicity of 5-MeO-DMT

Like all molecules 5-MeO-DMT is toxic at a sufficiently high dose, although there never has been a reported human death from consumption of the drug alone. 5-MeO-DMT in mice has been estimated to be between 48 – 278 $mg.Kg^{-1}$; hyperthermia, ataxia, and convulsions are attributed to toxicity of the drug.[95] The active dose of 5-MeO-DMT administered to adult humans via hot-vapor inhalation or intravenous injection is 1 – 5 mg for an adult human, there is a wide therapeutic window.[96] However, we wished to determine if the NEs could protect cells from the effects of the drug, as they protect the drug from external stressors. This would suggest that nanoencapsulation could widen the therapeutic window even further.

We examined the concentration-dependent cytotoxicity of the two NE systems *vis-a-vis* the unformulated 5-MeO-DMT in three different human cancer (MDA-MB-231[97], U87 GBM, and

U251 GBM), and a non-cancerous rat (L2), cell line.[98] **Figure 8** shows, for all cell lines, the NEs were less toxic than the unformulated drug. Taking the generally accepted threshold of 80% viability being non-toxic,[99] the NEs were only toxic at 275 $\mu g \cdot g^{-1}$ in the U251 GBM cell line. The use of the GRAS ingredients in our formulations ensures that we can expect no incidental toxicity from excipients. The unformulated drug was toxic in all cell lines at the highest concentration. Further investigation is underway to examine routes of 5-MeO-DMT toxicity mitigation through the NEs.

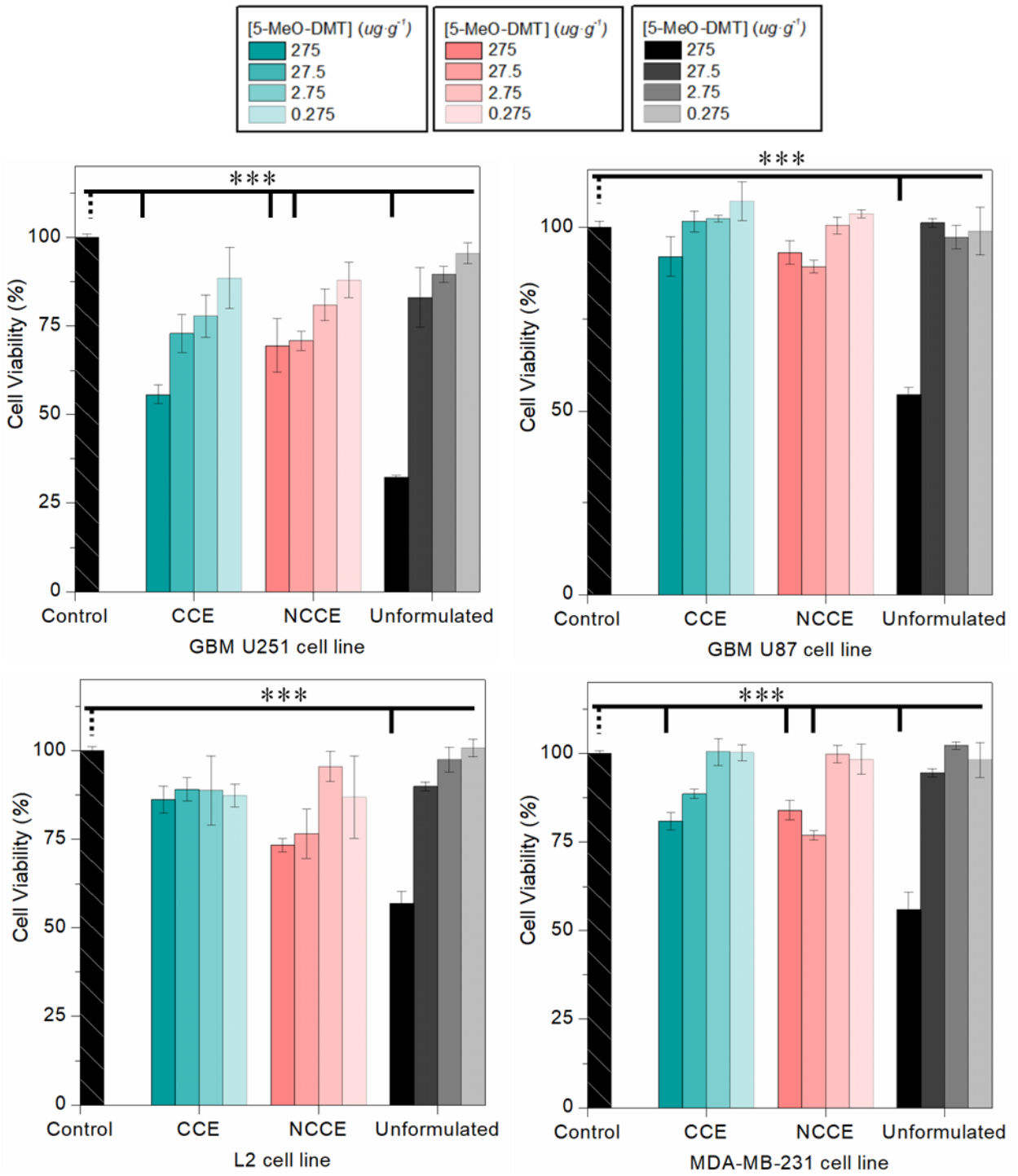

Figure 8. Cell viability upon dosing with CCE, NCCE, and unformulated 5-MeO-DMT. Initial [5-MeO-DMT] is 2.75 $mg{\cdot}g^{-1}$, molar concentration is *ca.* 25 *mM*. NCCE is in salmon, CCE is in teal, and black is the unformulated drug. Error bars represent standard deviation of three experimental replicates. Control is cells treated with only media. *** $P < 0.001$. Solid vertical lines indicate samples are identical to each other but significantly different from the hashed line.

The NEs facilitate uptake into the cells

We have established that the NEs protect the API from physical stressors likely to be encountered during processing and storage and have shown that they overcome the solubility problem of 5-MeO-DMT, but a third major reason to formulate is to assist in uptake across the blood-brain-barrier, essential for any central-nervous system active agent. This can be modelled through simple cell-uptake studies. The penetration of polar compounds through a cell membrane into live cells requires chemical support such as excipients used in formulations or cell-penetrating peptides;[100] this is even more important for therapeutic psychoactivity.[101],[102] To visualize the process, Nile Red was co-encapsulated within the NE along with 5-MeO-DMT. Results indicate that the CCE and NCCE formulations show delivery of the psychedelic payload through cell membranes of U87 glioblastoma (GBM) in fluorescence imaging by detection of the fluorophore (Nile Red) at the cells' nuclei (**Figure 9a**). To further confirmation of cell uptake of NEs, colocalization of them was evaluated by confocal laser scanning microscopy (**Figure 9b**). The occurrence of orange inside the cytoskeleton (green regions) and around the cell nuclei (blue regions) was evidence of NEs entering both GBM cell lines. These data were consistent with the fluorescence microscopy images mentioned above.

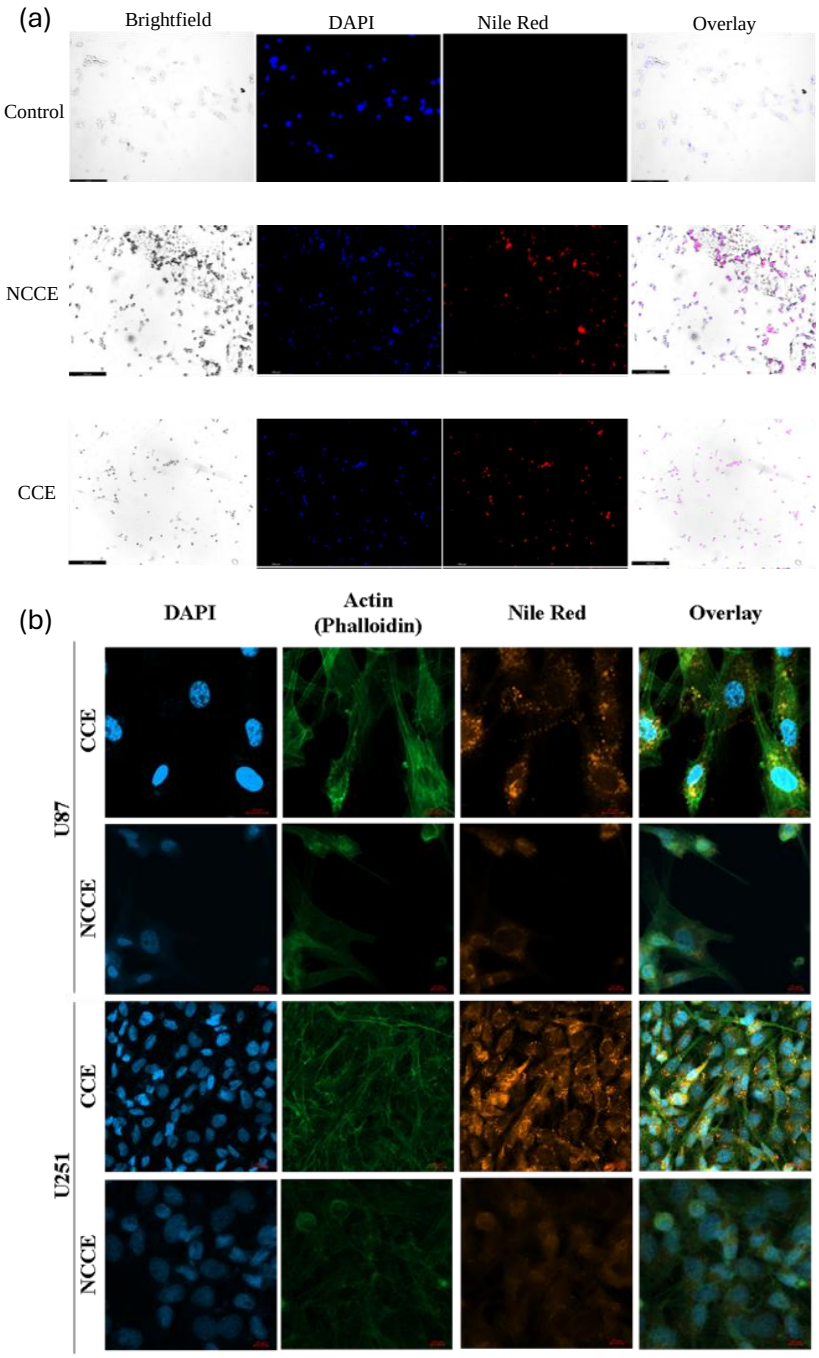

Figure 9. Cellular uptake of CCE and NCCE (a) Fluorescence microscopy images of U87 GBM cells. DAPI-stained cells exhibiting distinct nuclear outlines. The blue fluorescence indicates the location and distribution of nuclei within the population. The red fluorescence shows distribution of NEs doped with Nile Red. The overlay showed colocalization of NEs and nuclei. (scale bar for all images is 200 µm, contrast has been increased by 40% of the original image). (b) Confocal

laser scanning microscopy images of intracellular trafficking of the NEs doped with Nile Red on U87 and U251 GBM cells. The nucleus and cytoskeleton were stained with DAPI (blue) and phalloidin (green), respectively. The orange localized the distribution of NEs doped with Nile Red. The overlay showed colocalization of NEs around nuclei and inside the cells. (scale bar for all images is mentioned on them).

The NEs are compatible carriers with the ability to significantly improve the uptake of poorly soluble APIs such as 5-MeO-DMT. The use of HP – GTP_{noncov} and HP – GTP_{cov} offers several advantages, including enhanced solubility, stability, and cellular uptake; furthermore, it is known that natural polypeptides function as shuttles enabling the influx of a varied range of small molecules across the BBB.[103] NEs with average droplet sizes under 200 nm show enhanced cellular uptake of the bioactive and increased bioavailability for bioactive payloads such as paclitaxel,[104] candesartan cilexetil,[105] curcumin,[106] quercetin,[107] and resveratrol.[108] Recent reviews have highlighted that this uptake activity is not dependent on the supposed enhanced permeability and retention effect,[109] which despite justifications in the literature, is well-established to not be a meaningful mechanism in humans (although it does exist in rodents).[110, 111] Further *in vivo* or *ex vivo* studies are required to evaluate the NEs' ability to cross blood-brain barrier (BBB) and delivery of psychotherapeutics to the brain.

Conclusion

Functionalized DMT-based psychedelics are recent additions to the pharmacopeia for the treatment of multiple disorders affecting the brain and the nervous system. Very little research has been done (or at any rate published) on formulations designed to overcome the limitations associated with the administration of psychedelics in a dose-controlled format; in fact, based on registered clinical trials, it appears the industry has not considered the need to move towards nanoencapsulation to ensure controlled delivery of a specific dose. Our *de novo* emulsifiers with antioxidant properties form stable, robust 5-MeO-DMT formulations. Not only do these drug delivery vehicles protect the API from oxidative degradation, but they also lead to a high cellular uptake with reduced cytotoxicity of the API. These NEs with secondary antioxidant properties might be readily customized for oral and trans-buccal as well as intranasal delivery, providing simple routes of administration for psychopharmaceuticals and favoring patient compliance due

to their ease of use, comfort, and cost-effectiveness. This is the first of a series of reports on the application of nanoscience and technology in the targeted delivery of psychoactive APIs. These neoteric emulsifiers behave as 'Trojan horses', carrying the API payload to intracellular destinations inaccessible to the unformulated APIs.[112],[113] We hope that these formulations will eventually benefit vulnerable populations living with mental health disorders, as the scientific community re-examines tryptamines and their derivatives as an oft-overlooked class of drugs.

Supporting Information

The supporting information accompanying the article includes additional figures and details on the characterization of both the basic conjugates and the drug-loaded nanoemulsions, additional details on the experimental methods, spectral data and characterization information on the 5-MeO-DMT used in the study, additional figures showing the effect of physical stressors on the formulations, and the mathematical modelling of the kinetic release data. Specific figures, discussions, and protocols are referred to at the appropriate point in the manuscript to simplify navigation.

Author Contributions

Conceptualization, JFT, ARB, JS; Funding acquisition JFT; Investigation — Chemical synthesis, AH; Investigation — Formulation and Characterization, WCH, KR, ARB; Investigation — Biology, BB, KD; Investigation — Analytical chemistry, MAE, AK; Methodology, JFT, WCH, ARB, KD, BB, MAE; Visualization, WCH, ARB, BB, KD; Project administration, JFT, JS; Supervision, JFT; Writing — original draft, WCH, ARB, KR; Writing — review and editing, All authors.

Regulatory Statement

5-MeO-DMT is not a regulated substance in Canada where this work took place. The 5-MeO-DMT used in this study was synthesized in the lab for use in these formulation studies. John Trant and the University of Windsor hold research exemptions from Health Canada (55193.12.22, 55194.12.22, 55195.12.22) to conduct research with selected regulated psychedelics that are otherwise controlled substances and illegal for possession and use in Canada.

Conflict of Interest Statement

The Huxley Group holds a provisional patent (USPTO application #63/437,448) and has filed a full patent protecting this innovation. Drs. Trant, Banerjee, Simone, and Will Hosie are inventors. The Huxley Group was involved with planning the initial direction of this research, but had no input into the specific methodologies employed, nor did they have any input or access to limit or influence the results or conclusions of the work. Huxley was provided with a draft of this manuscript prior to submission for information purposes to ensure that no additional IP action was needed. No changes were requested or made to the manuscript. Dr. Simone participated as an author independent of his role as an executive of the Huxley Group during the time the work was completed.

JFT is the CEO of Binary Star Research Services (BSRS). BSRS has no input into this project and has no commercial interest in the subject of this work. BSRS holds no IP on this project, nor did it provide or receive any funding associated with this work.

Acknowledgements

The authors would like to thank the Natural Sciences and Engineering Research Council of Canada (RGPIN-2024-04113, ALLRP 586083 – 23 to JFT) for funding this work. The latter grant is also co-funded by MITACS through the Accelerate program (IT31979) and the Huxley Group. Thank you to Great Lakes Institute of Environmental Research (GLIER) for access to their scanning electron microscope, as well as the University of Western Ontario for access to their circular dichroism instrument. Biorender was used to create the graphical abstract.

References

1. Cristino, L.; Bisogno, T.; Di Marzo, V., *Nat. Rev. Neurol.* **2020,** *16* (1), 9-29.
2. García-Gutiérrez, M. S.; Navarrete, F.; Gasparyan, A.; Austrich-Olivares, A.; Sala, F.; Manzanares, J., *Biomolecules* **2020,** *10* (11), 1575.
3. Goldberg, S. B.; Pace, B. T.; Nicholas, C. R.; Raison, C. L.; Hutson, P. R., *Psychiatry Res.* **2020,** *284*, 112749.
4. Vamvakopoulou, I. A.; Narine, K. A. D.; Campbell, I.; Dyck, J. R. B.; Nutt, D. J., *Neuropharmacology* **2023,** *222*, 109294.
5. James, E.; Erritzoe, D.; Benway, T.; Joel, Z.; Timmermann, C.; Good, M.; Agnorelli, C.; Weiss, B. M.; Barba, T.; Campbell, G.; Baker Jones, M.; Hughes, C.; Topping, H.; Boyce, M.; Routledge, C., *Front. Psychiatry* **2024,** *14*.

6. Aicher, H. D.; Mueller, M. J.; Dornbierer, D. A.; Suay, D.; Elsner, C.; Wicki, I.; Meling, D.; Caflisch, L.; Hempe, A.; Steinhart, C.; Mueller, J.; Von Rotz, R.; Kleim, B.; Scheidegger, M., *Front. Psychiatry* **2024,** *14*.
7. Carbonaro, T. M.; Gatch, M. B., *Brain Res. Bull.* **2016,** *126* (Pt 1), 74-88.
8. Barker, S. A., *Psychopharmacology* **2022,** *239* (6), 1749-1763.
9. dos Santos, R. G.; Hallak, J. E. C., *Epilepsy Behav.* **2021,** *121*, 106300.
10. Sommano, S. R.; Chittasupho, C.; Ruksiriwanich, W.; Jantrawut, P., *Molecules* **2020,** *25* (24), 5792.
11. Leinen, Z. J.; Mohan, R.; Premadasa, L. S.; Acharya, A.; Mohan, M.; Byrareddy, S. N., *Biomedicines* **2023,** *11* (10).
12. Sampson, P. B., *J. Nat. Prod* **2021,** *84* (1), 142-160.
13. Koltai, H.; Namdar, D., *Tr. Plant Sci.* **2020,** *25* (10), 976-984.
14. Holze, F.; Liechti, M. E.; Hutten, N.; Mason, N. L.; Dolder, P. C.; Theunissen, E. L.; Duthaler, U.; Feilding, A.; Ramaekers, J. G.; Kuypers, K. P. C., *Clin. Pharmacol. Ther.* **2021,** *109* (3), 658-666.
15. Inserra, A.; Piot, A.; De Gregorio, D.; Gobbi, G., *CNS Drugs* **2023,** *37* (9), 733-754.
16. Voineskos, D.; Daskalakis, Z. J.; Blumberger, D. M., *Neuropsychiatr. Dis. Treat.* **2020,** *16*, 221-234.
17. Aleksandrova, L. R.; Phillips, A. G., *Tr. Pharmcol. Sci* **2021,** *42* (11), 929-942.
18. De Gregorio, D.; Aguilar-Valles, A.; Preller, K. H.; Heifets, B. D.; Hibicke, M.; Mitchell, J.; Gobbi, G., *J. Neurosci.* **2021,** *41* (5), 891-900.
19. Mertens, L. J.; Preller, K. H., *Pharmacopsychiatry* **2021,** *54* (04), 176-190.
20. DiVito, A. J.; Leger, R. F., *Mol. Biol. Rep.* **2020,** *47* (12), 9791-9799.
21. McClure-Begley, T. D.; Roth, B. L., *Nat. Rev. Drug Discov.* **2022,** *21* (6), 463-473.
22. Martins, D.; Gil-Martins, E.; Cagide, F.; da Fonseca, C.; Benfeito, S.; Fernandes, C.; Chavarria, D.; Remião, F.; Silva, R.; Borges, F., *Pharmaceuticals* **2023,** *16* (8), 1158.
23. Dourron, H. M.; Nichols, C. D.; Simonsson, O.; Bradley, M.; Carhart-Harris, R.; Hendricks, P. S., *Psychopharmacology* **2023,** *Ahead of Print*.
24. Reckweg, J. T.; Uthaug, M. V.; Szabo, A.; Davis, A. K.; Lancelotta, R.; Mason, N. L.; Ramaekers, J. G., *J. Neurochem.* **2022,** *162* (1), 128-146.
25. Lima da Cruz, R. V.; Moulin, T. C.; Petiz, L. L.; Leão, R. N., *Front. Mol. Neurosci.* **2018,** *11*.
26. Lima da Cruz, R. V.; Moulin, T. C.; Petiz, L. L.; Leão, R. N., *Front. Mol. Neurosci.* **2019,** *12*.
27. Nogueira, M.; Ferreira Golbert, D. C.; Menezes, R.; Nóbrega de Almeida, R.; Galvão-Coelho, N. L.; Siroky, A. N.; Lima, T. Z.; Maia, H.; Leão, K. E.; Leão, R. N., *Mol. Psychiatry* **2025,** *30* (1), 50-60.
28. Reckweg, J. T.; van Leeuwen, C. J.; Henquet, C.; van Amelsvoort, T.; Theunissen, E. L.; Mason, N. L.; Paci, R.; Terwey, T. H.; Ramaekers, J. G., *Front. Psychiatry* **2023,** *14*, 1133414.
29. Rucker, J. J.; Roberts, C.; Seynaeve, M.; Young, A. H.; Suttle, B.; Yamamoto, T.; Ermakova, A. O.; Dunbar, F.; Wiegand, F., *J. Psychopharmacol.* **2024,** *38* (8), 712-723.
30. O' Donovan, D. H.; De Fusco, C.; Kuhnke, L.; Reichel, A., *J. Med. Chem.* **2023,** *66* (4), 2347-2360.
31. Costa, C. P.; Moreira, J. N.; Sousa Lobo, J. M.; Silva, A. C., *Acta Pharm. Sin. B* **2021,** *11* (4), 925-940.

32. Mustafa, G.; Alrohaimi, A. H.; Bhatnagar, A.; Baboota, S.; Ali, J.; Ahuja, A., *Drug Deliv.* **2014,** *23* (3), 923-929.
33. Hanson, L. R.; Frey, W. H., 2nd, *BMC Neurosci.* **2008,** *9 Suppl 3* (Suppl 3), S5-S5.
34. Won, S.; An, J.; Song, H.; Im, S.; You, G.; Lee, S.; Koo, K.-i.; Hwang, C. H., *Front. Neurosci.* **2023,** *17*.
35. Henriques, P.; Fortuna, A.; Doktorovová, S., *Eur. J. Pharm. Biopharm.* **2022,** *176*, 1-20.
36. Dalgleish, D. G., *Tr. Food Sci. Technol.* **1997,** *8* (1), 1-6.
37. Zhang, M.; Fan, L.; Liu, Y.; Huang, S.; Li, J., *Food Chem.* **2022,** *397*, 133726.
38. Ma, K. K.; Greis, M.; Lu, J.; Nolden, A. A.; McClements, D. J.; Kinchla, A. J., *Foods* **2022,** *11* (4), 594.
39. Kim, W.; Wang, Y.; Selomulya, C., *Tr. Food Sci. Technol.* **2020,** *105*, 261-272.
40. Tan, M.; Nawaz, M. A.; Buckow, R., *Food Rev. Int.* **2023,** *39* (5), 2428-2456.
41. Lima, R. R.; Stephani, R.; Perrone, Í. T.; de Carvalho, A. F., *Food Chem. Adv.* **2023,** *3*, 100397.
42. Mota da Silva, A. M.; Souza Almeida, F.; Kawazoe Sato, A. C., *J. Food Eng.* **2021,** *292*, 110277.
43. Cory, H.; Passarelli, S.; Szeto, J.; Tamez, M.; Mattei, J., *Front. Nutr.* **2018,** *5*, 87.
44. Rasouli, H.; Farzaei, M. H.; Khodarahmi, R., *Int. J. Food Prop.* **2017,** *20* (sup2), 1700-1741.
45. Elzoghby, A. O.; Samy, W. M.; Elgindy, N. A., *J. Controlled Release* **2012,** *161* (1), 38-49.
46. Ismail, R.; Baaity, Z.; Csóka, I., *Drug Discov. Today* **2021,** *26* (8), 1929-1935.
47. Vasava, H.; Singh, R.; Yadav, T., *Int. J. Dairy Technol.* **2022,** *75* (3), 563-574.
48. Tazeddinova, D., Toshev, A. D., Abylgazinova, A., Rahman, M., Matin, M., Bin Bakri, M. K., and Ayan, O., *BioResources* **2022,** *17* (4), 6997-7030.
49. Parolia, S.; Maley, J.; Sammynaiken, R.; Green, R.; Nickerson, M.; Ghosh, S., *Food Chem.* **2021,** *367*, 130603.
50. Padial-Domínguez, M.; Espejo-Carpio, F. J.; Pérez-Gálvez, R.; Guadix, A.; Guadix, E. M., *Foods* **2020,** *9* (5), 636.
51. Hou, Z.; Gao, Y.; Yuan, F.; Liu, Y.; Li, C.; Xu, D., *J. Agric. Food Chem.* **2010,** *58* (15), 8604-8611.
52. Lim, S.; Salentinig, S., *Curr. Opin. Colloid Interface Sci.* **2021,** *56*, 101485.
53. To the reviewer: the synthesis is proprietary and being patented. We expect it to be at least available as a ChemRxiv by the time of publication, and this note will be replaced. Regardless, spectral data is provided in the SI of this paper to provide confidence in the material being used. In the case that this article publishes before a reference is available, the spectral data will note that it was compared to a literature reference with an alternative synthesis of 5-MeO-DMT to ensure a reader can replicate the study.
54. Chatterjee, R.; Dey, T. K.; Ghosh, M.; Dhar, P., *Food Bioprod. Proces.* **2015,** *94*, 70-81.
55. Banerjee, A.; Binder, J.; Salama, R.; Trant, J. F., *J. Cannabis Res.* **2021,** *3* (1), 43.
56. Etzbach, L.; Stolle, R.; Anheuser, K.; Herdegen, V.; Schieber, A.; Weber, F., *Antioxidants (Basel)* **2020,** *9* (6).
57. Vistica, D. T.; Skehan, P.; Scudiero, D.; Monks, A.; Pittman, A.; Boyd, M. R., *Cancer Res.* **1991,** *51* (10), 2515-2520.
58. Sood, S.; Jawahar, N.; Jain, K.; Kuppusamy, G.; S.N, M., *Curr. Nanosci.* **2013,** *9*, 26-34.

59. Zielińska, A.; da Ana, R.; Fonseca, J.; Szalata, M.; Wielgus, K.; Fathi, F.; Oliveira, M. B. P. P.; Staszewski, R.; Karczewski, J.; Souto, E. B., *Molecules* **2023,** *28* (6), 2875.
60. Armstrong, R. A., *Ophthal. Physiol. Optics* **2014,** *34* (5), 502-508.
61. Liu, J.; Yong, H.; Yao, X.; Hu, H.; Yun, D.; Xiao, L., *RSC Adv.* **2019,** *9* (61), 35825-35840.
62. Wang, X.; Feng, Y.; Chen, C.; Yang, H.; Yang, X., *LWT* **2020,** *131*, 109810.
63. Ricci, L.; Umiltà, E.; Righetti, M. C.; Messina, T.; Zurlini, C.; Montanari, A.; Bronco, S.; Bertoldo, M., *J. Sci. Food Agr.* **2018,** *98* (14), 5368-5377.
64. Yang, G.; Bao, Y.; Sun, K.-f.; Chang, C.; Liu, W.-f., *Food Hydrocoll.* **2020,** *112*, 106293.
65. Pan, X.; Fang, Y.; Wang, L.; Shi, Y.; Xie, M.; Xia, J.; Pei, F.; Li, P.; Xiong, W.; Shen, X.; Hu, Q., *J. Agr. Food Chem.* **2019,** *67* (14), 4023-4030.
66. Liu, F.; Ma, C.; McClements, D. J.; Gao, Y., *Food Hydrocoll.* **2017,** *63*, 625-634.
67. Meng, Y.; Li, C., *Food Chem.* **2021,** *364*, 129622.
68. Parolia, S.; Maley, J.; Sammynaiken, R.; Green, R.; Nickerson, M.; Ghosh, S., *Food Chem.* **2022,** *367*, 130603.
69. Vivian, J. T.; Callis, P. R., *Biophys. J.* **2001,** *80* (5), 2093-2109.
70. Micsonai, A.; Moussong, É.; Wien, F.; Boros, E.; Vadászi, H.; Murvai, N.; Lee, Y.-H.; Molnár, T.; Réfrégiers, M.; Goto, Y.; Tantos, Á.; Kardos, J., *Nucl. Acids Res.* **2022,** *50* (W1), W90-W98.
71. Sharon, M. K.; Nicholas, C. P., *Curr. Prot. Pept. Sci.* **2000,** *1* (4), 349-384.
72. Aryee, A. N. A.; Agyei, D.; Udenigwe, C. C., 2 - Impact of processing on the chemistry and functionality of food proteins. In *Proteins in Food Processing (Second Edition)*, Yada, R. Y., Ed. Woodhead Publishing: 2018; pp 27-45.
73. Agustinisari, I.; Mulia, K.; Harimurti, N.; Nasikin, M.; Rienoviar; Herawati, H.; Manalu, L. P., *Int. J. Food Sci.* **2024,** *2024* (1), 3254132.
74. Annan, W. S.; Fairhead, M.; Pereira, P.; Walle, C. F. v. d., *Protein Eng. Des. Sel.* **2006,** *19* (12), 537-545.
75. Li, Y.; Wang, H.; Zhao, Y.; Chen, Q.; Xia, X.; Liu, Q.; Kong, B., *Foods* **2024,** *13* (2), 253.
76. Tsujikawa, K.; Kuwayama, K.; Miyaguchi, H.; Kanamori, T.; Iwata, Y. T.; Inoue, H., *Forensic Sci. Int.* **2009,** *193* (1), 106-111.
77. Shen, H.-W.; Jiang, X.-L.; C. Winter, J.; Yu, A.-M., *Curr. Drug Metab.* **2010,** *11* (8), 659-666.
78. Sherwood, A. M.; Claveau, R.; Lancelotta, R.; Kaylo, K. W.; Lenoch, K., *ACS Omega* **2020,** *5* (49), 32067-32075.
79. Mishra, K.; Ojha, H.; Chaudhury, N. K., *Food Chem.* **2012,** *130* (4), 1036-1043.
80. Munteanu, I. G.; Apetrei, C., *Int. J. Mol. Sci.* **2021,** *22* (7), 3380.
81. de Camargo, A. C.; Biasoto, A. C. T.; Schwember, A. R.; Granato, D.; Rasera, G. B.; Franchin, M.; Rosalen, P. L.; Alencar, S. M.; Shahidi, F., *Food Chem.* **2019,** *290*, 229-238.
82. Foti, M. C., *J. Agric. Food Chem.* **2015,** *63* (40), 8765-8776.
83. Rahman, M. M.; Islam, M. B.; Biswas, M.; Khurshid Alam, A. H. M., *BMC Res. Notes* **2015,** *8* (1), 621.
84. Mao, L.; Wang, D.; Liu, F.; Gao, Y., *Crit. Rev. Food Sci. Nutr.* **2018,** *58* (5), 770-784.
85. McClements, D. J., *Food Emulsions: Principles, Practices, and Techniques*. CRC press: **2004**.
86. McClements, D. J., *Curr. Opin. Colloid Interface Sci.* **2004,** *9* (5), 305-313.
87. Al-Jumaily, A.; Meshkinzar, A.; Torres, L., *Food Eng. Rev.* **2023,** *15*, 1-15.
88. Demetriades, K.; Coupland, J. N.; McClements, D., *J. Food Sci.* **2006,** *62*, 342-347.

89. Keowmaneechai, E.; McClements, D., *J. Food Sci.* **2002,** *67*, 665-671.
90. Ralla, T.; Salminen, H.; Edelmann, M.; Dawid, C.; Hofmann, T.; Weiss, J., *Food Biophys.* **2017,** *12* (3), 269-278.
91. Chung, C.; Sher, A.; Rousset, P.; McClements, D. J., *Food Res. Int.* **2017,** *99*, 770-777.
92. Li, M.; Ritzoulis, C.; Du, Q.; Liu, Y.; Ding, Y.; Liu, W.; Liu, J., *Front. Nutr.* **2021,** *8*.
93. Morakul, B.; Teeranachaideekul, V.; Limwikrant, W.; Junyaprasert, V. B., *Sci. Rep.* **2024,** *14* (1), 8851.
94. Miastkowska, M.; Sikora, E.; Ogonowski, J.; Zielina, M.; Łudzik, A., *Colloids Surf. A Physicochem. Eng. Asp.* **2016,** *510*, 63-68.
95. Shen, H. W.; Jiang, X. L.; Yu, A. M., *Drug Metab. Dispos.* **2011,** *39* (7), 1227-34.
96. Shulgin, A. T.; Shulgin, A., *Tihkal : the continuation*. 1st ed.; Transform Press: Berkeley, CA, **1997**.
97. Cailleau, R.; Olivé, M.; Cruciger, Q. V. J., *In Vitro* **1978,** *14* (11), 911-915.
98. Shi, M. M.; Kugelman, A.; Iwamoto, T.; Tian, L.; Forman, H. J., *J. Biol. Chem.* **1994,** *269* (42), 26512-7.
99. Tests for *in vitro* Cytotoxicity. In *Biological Evaluation of Medical Devices*, ISO: Geneva, Switzerland, **2009**; Vol. 10993-5.
100. Reissmann, S., *J. Pept. Sci.* **2014,** *20* (10), 760-784.
101. Nogueira, C.; Lemos-Senna, E.; da Silva Vieira, E.; Sampaio, T. B.; Mallmann, M. P.; Oliveira, M. S.; Bernardi, L. S.; Oliveira, P. R., *J. Nanopart. Res.* **2023,** *25* (1), 19.
102. Costa, C.; Moreira, J. N.; Amaral, M. H.; Sousa Lobo, J. M.; Silva, A. C., *J. Controlled Release* **2019,** *295*, 187-200.
103. Peng, X.; Liu, X.; Kim, J. Y.; Nguyen, A.; Leal, J.; Ghosh, D., *Bioconjugate Chem.* **2023,** *34* (12), 2319-2336.
104. Choudhury, H.; Gorain, B.; Karmakar, S.; Biswas, E.; Dey, G.; Barik, R.; Mandal, M.; Pal, T. K., *Int. J. Pharm. (Amsterdam, Neth.)* **2014,** *460* (1), 131-143.
105. Gao, F.; Zhang, Z.; Bu, H.; Huang, Y.; Gao, Z.; Shen, J.; Zhao, C.; Li, Y., *J. Controlled Release* **2011,** *149* (2), 168-174.
106. Simion, V.; Stan, D.; Constantinescu, C. A.; Deleanu, M.; Dragan, E.; Tucureanu, M. M.; Gan, A.-M.; Butoi, E.; Constantin, A.; Manduteanu, I.; Simionescu, M.; Calin, M., *J. Pharm. Pharmacol.* **2016,** *68* (2), 195-207.
107. Chen, W.; Ju, X.; Aluko, R. E.; Zou, Y.; Wang, Z.; Liu, M.; He, R., *Food Hydrocoll.* **2020,** *108*, 106042.
108. Sessa, M.; Balestrieri, M. L.; Ferrari, G.; Servillo, L.; Castaldo, D.; D'Onofrio, N.; Donsì, F.; Tsao, R., *Food Chem.* **2014,** *147*, 42-50.
109. Ganta, S.; Deshpande, D.; Korde, A.; Amiji, M., *Mol. Membr. Biol.* **2010,** *27* (7), 260-273.
110. Danhier, F., *J. Controlled Release* **2016,** *244*, 108-121.
111. Nichols, J. W.; Bae, Y. H., *J. Controlled Release* **2014,** *190*, 451-464.
112. Gabizon, A.; Papahadjopoulos, D., *Proc. Natl. Acad. Sci. U. S. A.* **1988,** *85* (18), 6949-53.
113. Hillaireau, H.; Couvreur, P., *Cell. Mol. Life Sci.* **2009,** *66* (17), 2873-96.